Chemistry & Biology, Vol. 10, 1023–1032, November, 2003, ©2003 Elsevier Science Ltd. All rights reserved. DOI 10.1016/j.chembiol.2003.10.009

Cooperativity, Partially Bound States, and Enthalpy-Entropy Compensation

Christopher A. Hunter* and Salvador Tomas
Centre for Chemical Biology
Krebs Institute for Biomolecular Science
Department of Chemistry
University of Sheffield
Sheffield S3 7HF
United Kingdom

Summary

Efforts to develop a quantitative understanding of molecular recognition rely on the additivity of individual intermolecular interactions, and cooperativity represents one of the major potential stumbling blocks. A chemical double-mutant cycle has been used to experimentally measure cooperativity between functional group interactions within a complex framework. The interaction between two aromatic groups varies by 0.2 ± 0.4 kJ mol^{-1} in synthetic H-bonded complexes that differ by 8–13 kJ mol^{-1} in overall stability. In these systems, the free energies associated with individual intermolecular interactions can therefore be reliably treated in an additive fashion. The results suggest that alternative explanations should be considered for cooperative phenomena observed in other systems, and a rationale based on the population of partially bound states in flexible molecules is proposed to account for the enthalpic chelate effect and enthalpy-entropy compensation.

Introduction

In systems that feature multiple intermolecular interactions, the free energy contribution that an individual interaction makes to the stability of an assembly as a whole can be significantly larger than one might expect based on the properties of that interaction studied in isolation [1, 2]. In other words, a complex that makes two intermolecular interactions may be associated with a free energy of formation more than twice as large as a similar complex that makes one interaction. This phenomenon is termed cooperativity, strictly positive cooperativity. It was first studied in detail by coordination chemists, who coined the term chelate effect for the enhanced coordinating properties of multivalent ligands [3–5]. This classical chelate effect is based on entropy: if multiple interaction sites are anchored on a single molecule, the entropic penalty associated with formation of a bimolecular complex is removed by the first interaction formed, and all subsequent interactions are therefore enhanced. There are also enthalpic effects that can lead to cooperativity: changes in electronic structure or conformation caused by one interaction can stabilize subsequent interactions [6–14].

Recently, Williams suggested another more general phenomenon that could give rise to enthalpic cooperativity [15–18]. The idea of the enthalpic chelate effect is that in a complex that is held together by multiple weak noncovalent interactions, the enthalpy of all of the individual intermolecular bonding interactions is weakened by extensive intermolecular motion (Figure 1). If additional interaction sites are added to generate a more strongly bound complex, the intermolecular motion is damped, and all of the individual interactions become more favorable. An attractive feature of this model is that it also explains the phenomenon of enthalpy-entropy compensation [19–22]. Experimentally, it is found that the entropy and the enthalpy of intermolecular complexation compensate each other, and the trade-off between intermolecular motion and enthalpic interactions discussed above accounts for this general observation. The Williams model of enthalpic cooperativity has important implications for understanding molecular recognition events at a quantitative level, because if cooperative effects are significant and widespread, the strength of any given intermolecular interaction will depend critically on the context in which it is found.

We have been using chemical double-mutant cycles to quantify aromatic interactions, and a key assumption in our approach is that the free energies of intermolecular interactions are additive to a first approximation [23–26]. The double-mutant cycle approach is illustrated in Figure 2A. In principle, an estimate of the interaction between functional groups **i** and **j** could be obtained by comparing the free energies of formation of complexes *A* and *B*. Here, the **i-j** interaction is the free energy contribution that **i** and **j** make to the stability of complex *A*, after the entropic penalty associated with biomolecular complexation has been removed by the other interactions in the core of complex *A*. However, the difference between the stabilities of complexes *A* and *B* measures not only the **i-j** interaction; it also includes a contribution from secondary interactions between **i** and the core of the complex, as illustrated in Figure 2A. These secondary interactions can be measured directly by comparing the free energies of complexes *C* and *D*, and so the **i-j** interaction can be quantified as:

$$\Delta\Delta G_{i\text{-}j} = \Delta G_A - \Delta G_B - \Delta G_C + \Delta G_D. \quad (1)$$

An important feature of this approach is that many systematic errors cancel, because each compound used appears in two complexes, and it is the difference in free energies that is used. Thus, potential errors associated with aggregation of the components, additional conformational equilibria, and minor conformational differences in the free or bound states are all effectively removed. However, if the free energy contribution of a single functional group interaction changes significantly between a weakly and a strongly bound complex, the approach is not valid. For example, if there are large cooperative effects, the secondary interactions measured using the weakly bound complexes *C* and *D* would be significantly less than the secondary interactions

*Correspondence: c.hunter@sheffield.ac.uk

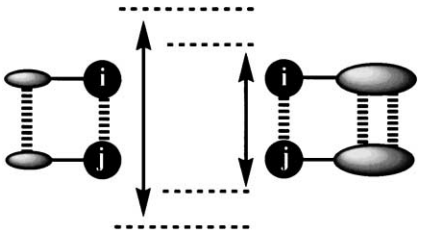

Figure 1. The Enthalpic Chelate Effect

In a weakly bound complex (left), there are large intermolecular motions, so that on average the interacting functional groups **i** and **j** are further apart than in a strongly bound complex (right). This structural tightening in strongly bound complexes leads to enthalpy-entropy compensation.

present in the strongly bound complexes *A* and *B*, and Equation 1 would not hold.

In order to test this hypothesis experimentally, we developed the chemical triple-mutant box (Figure 2B) [27]. This provides a tool for directly measuring cooperativity between intermolecular interactions. Complexes *A–D* constitute a double-mutant cycle to quantify the **i-j** interaction, as described above. Complexes *A′–D′* constitute a second double-mutant cycle to measure the same **i-j** interaction, but in this case the core of the complex is more strongly bound. Thus, the difference between the **i-j** interaction in the two double-mutant cycles allows us to directly measure how changing the overall stability of a complex affects the free energy contribution of individual intermolecular interactions. The eight complexes constitute a triple-mutant box, and the cooperativity between the additional interactions in the core of the complex and the **i-j** interaction is defined as:

$$\Delta\Delta G_{coop} = (\Delta G_{A'} - \Delta G_{B'} - \Delta G_{C'} + \Delta G_{D'}) - (\Delta G_A - \Delta G_B - \Delta G_C + \Delta G_D). \quad (2)$$

In the zipper complexes that we reported previously, no cooperativity was observed using this approach, but the **i-j** interaction was an aromatic interaction worth only 3 kJ mol^{-1}. It is likely that any cooperative effects would be buried in the experimental error (0.5 kJ mol^{-1}), so here we extend the method to significantly larger interaction energies.

A major disadvantage of the triple-mutant box approach is that accurate measurements are required on eight different complexes, and, practically, this is not easy to achieve. However, the measurement of cooperativity does not require the isolation a single functional group interaction. The change in a set of interactions can provide the same information, so one side of the triple-mutant box involving only four complexes is sufficient for our purposes. In other words, the four complexes that represent the front and back faces of the box in Figure 2B can be used to quantify functional group interaction energies, as described above, but the other four faces of the box can all be used to quantify cooperativity. In this case, we use complexes *A* and *C* to measure the sum of the interactions made by **j** with the rest of the complex, and we use complexes A′ and C′ to measure the same sum in a more strongly bound complex. Thus, the cooperativity is given by:

$$\Delta\Delta G_{coop} = \Delta G_{A'} - \Delta G_{C'} - \Delta G_A + \Delta G_C. \quad (3)$$

The system that we have realized for this purpose is illustrated in Figure 2C. For practical reasons, we make changes to both components of the complex, but the principles elaborated above for the construction of the *A-C-A′-C′* double-mutant cycle to quantify cooperativity still hold. This system provides us with complexes that are sufficiently stable to measure stability constants accurately, and the differences in free energy of complexation should be sufficiently large to detect any significant cooperativity.

Results

The synthesis of compounds **3, 4**, and **6–13** has been described elsewhere [23, 26, 27]. Compound **1** was obtained by coupling **9** with 4-*t*-butyl benzoyl chloride, followed by reaction with freshly prepared 4-nitro-pyrrole-2-carbonyl chloride **10**. Compound **2** was obtained by coupling isophthaloyl dichloride with **11**, followed by capping with freshly prepared 2,6-diisopropyl-*N,N*-dimethyl-benzene-1,4-diamine **12**. Compound **5** was obtained by coupling **13** with 4-*t*-butyl benzoyl chloride (Figure 3).

All of the compounds dimerize to some extent in chloroform, and these equilibria were characterized using ^{1}H NMR dilution experiments and isothermal titration calorimetry (ITC) (Table 1). Where the compounds could be studied using both techniques, the dimerization constants (K_d) were consistent, but the values obtained by ITC were consistently slightly lower than those obtained by the ^{1}H NMR experiments.

Formation of the 1:1 complexes shown in Figure 2C was investigated using three different techniques because of the wide range of complex stabilities. Complexes **5•6** and **7•8** were characterized by ^{1}H NMR titrations and dilutions, and complexes **3•4** and **1•2** were characterized by ^{1}H NMR dilutions and isothermal titration calorimetry (Table 1). In each case, the data were fit to 1:1 binding isotherms that allowed for dimerization of the individual compounds (Table 1). Although there is a small variation between the association constants measured using the different techniques, the difference in free energy between two complexes studied using the same technique is very consistent. The double-mutant cycle removes the systematic errors associated with the use of a particular technique, provided complexes are compared in a pairwise fashion. The most reliable data were obtained from the titration experiments where better saturation was achieved, and we have therefore used the ^{1}H NMR titration data for **5•6** and **7•8** and the ITC data for **3•4** and **1•2** in construction of the double-mutant cycle. The conclusions are not significantly altered by using any combination of the association constants in Table 1.

The structures of the complexes in solution were characterized using the complexation-induced changes in

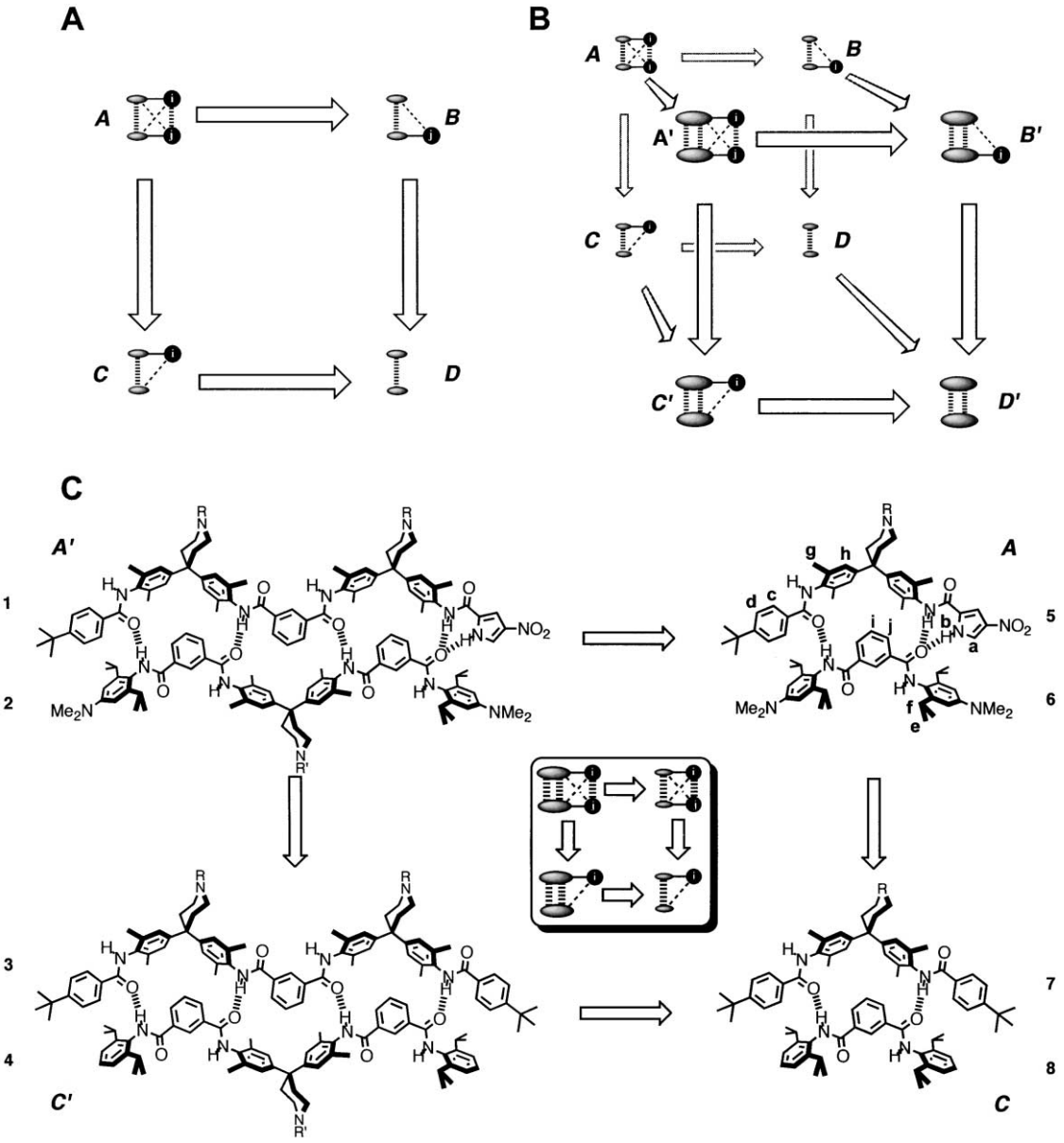

Figure 2. Chemical Double-Mutant Cycles and Triple-Mutant Boxes

(A) Schematic representation of the double-mutant cycle used to quantify the i-j interaction in complex A.

(B) Schematic representation of the triple-mutant box used to quantify cooperativity. The back face is identical to the double-mutant cycle in (A) and measures the i-j interaction in a weakly bound complex. The front face is a double-mutant cycle that measures the same interaction in a strongly bound complex. Cooperativity is measured as the change in the i-j interaction.

(C) A double-mutant cycle for measuring cooperativity. A cartoon representation of how this cycle relates to the corresponding triple mutant box is shown. The ^{1}H NMR labeling used in Table 2 is also illustrated.

chemical shift (CIS) (Table 2) and intermolecular NOEs from ROESY experiments (see Supplemental Data at http://www.chembiol.com/cgi/content/full/10/11/1023/DC1). The association constant of the **1•2** complex is too high to be measured using ^{1}H NMR titrations, but the CIS values could easily be determined from 1:1 mixtures that were fully bound. The CIS patterns are similar for all four complexes and are consistent with those reported previously for related zipper complexes. For example, the CIS values for the isophthaloyl triplets (i) are -1.7 ± 0.1 ppm, which locates this proton rather precisely in the same position in all four complexes. This shows that the chemical mutations do not significantly perturb the three-dimensional structures of the complexes, and differences is association constant can be attributed to changes in functional group interactions rather than conformational changes.

Using Equation 3 for the double-mutant cycle in Figure 2C gives a value of 0.2 ± 0.4 kJ mol^{-1} for the cooperativity in this system. Here, we are looking at changes in

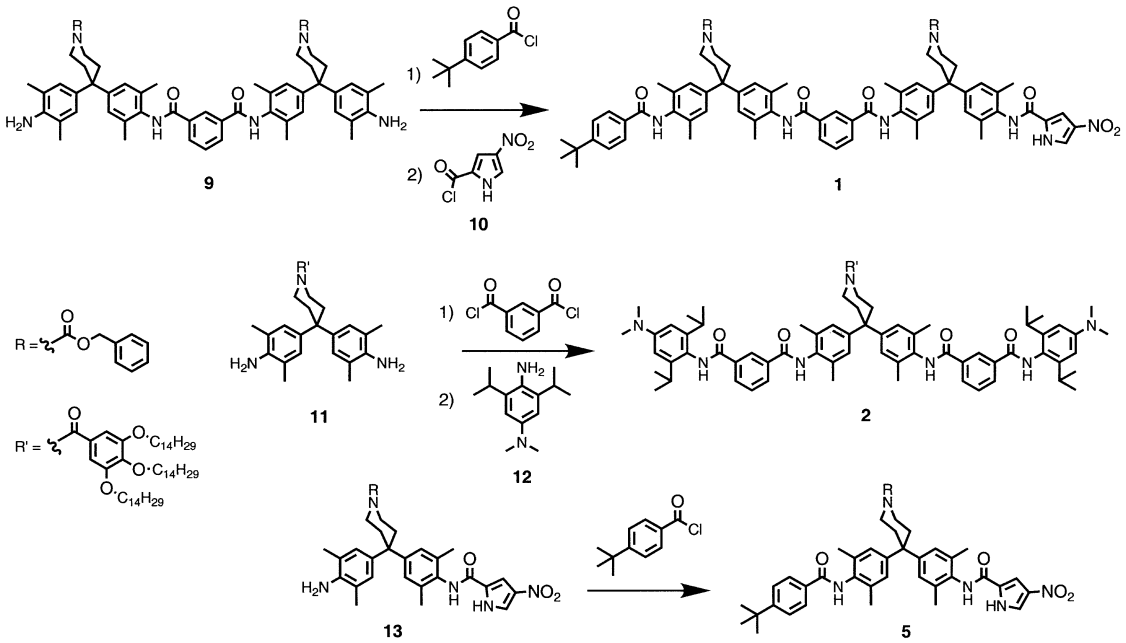

Figure 3. Synthesis of Compounds **1**, **2**, and **5**

interaction energy of 8–13 kJ mol^{-1}, a difference of four orders of magnitude between the stability constants of most weakly and strongly bound complexes, and the cooperativity is within the experimental error (0.4 kJ mol^{-1}).

Discussion

We could explain these results by suggesting that there are compensating unfavorable interactions in the tightly bound complexes that cancel out any cooperativity associated with structural tightening, or that structural tightening does not take place due to geometrical constraints. However, at the very least the experiments show that the free energy contribution of individual functional group interactions in the zipper systems is independent of the overall stability of the complex. This validates the double-mutant cycle approach to quantifying intermolecular interactions. This system represents only one example, but it does demonstrate that the enthalpic chelate effect is not a general phenomenon [28–31]. For the purposes of discussion, let's assume that this one example invalidates the model in Figure 1 and consider other possible explanations.

Experimental evidence for the enthalpic chelate effect comes from ^{1}H NMR experiments on vancomycin-peptide complexes [18]. The complexation-induced changes in chemical shift (CIS) report on the properties of individual intermolecular interactions at the binding interface, and as the overall stability of the complex increases, increases in the CIS values are observed. This suggests that as the overall stability of the complex increases, the structure tightens, and the individual interactions become more enthalpically favorable. There are clearly major differences between the vancomycin-peptide complexes and our zipper complexes, and this could help to rationalize both sets of experiments: one set of experiments was carried out in water, the other in

Table 1. Stability Constants (K, M^{-1}) and Free Energies of Complexation (ΔG, kJ mol^{-1}) in Chloroform at 294 K

Complex	K (NMR Titration)	K (NMR Dilution)	K (ITC Titration)	K (ITC Dilution)	ΔG
1$_2$		1100 ± 500		1070 ± 120	
2$_2$		280 ± 60		230 ± 25	
3$_2$		80 ± 20		72 ± 25	
4$_2$		420 ± 40		330 ± 20	
5$_2$		110 ± 30			
6$_2$		<5			
7$_2$		<5			
8$_2$		<5			
1•2		230,000 ± 40,000	175,000 ± 15,000		−29.5 ± 0.2[a]
3•4		10,500 ± 980	6500 ± 1000		−21.5 ± 0.3[a]
5•6	1100 ± 60	1020 ± 90			−17.1 ± 0.1[b]
7•8	38 ± 2	35 ± 4			−8.9 ± 0.1[b]

[a] Measured by ITC.
[b] Measured by ^{1}H NMR titration.

Table 2. Limiting Complexation-Induced Changes in ^{1}H NMR Chemical Shift (CIS in ppm) in $CDCl_3$ at 294 K

		Terminal Signals (at the Mutation Sites)						Core Signals			
Complex	NH	a	b	c	d	e	f	g	h	i	j
1•2[a]	[b]	−1.3	+2.1	−0.4	[b]	−0.1	0.0	0.0	+0.1	−1.7	[b]
								−0.1	+0.2	1.8	
3•4[a]	[b]			−0.3	−0.5	−0.1	0.0	0.0	+0.1	−1.6	−0.4
									+0.2	1.7	
5•6[b]	+2.6	−1.4	+2.0	−0.4	−0.5	−0.1	−0.1	0.0	+0.1	−1.7	−0.4
	+1.5							−0.1	+0.2		
	+0.6										
7•8[b]	+1.3			−0.3	−0.5	−0.1	0.0	0.0	+0.2	−1.6	−0.4
	+1.1										

[a] See Figure 2C for the proton labeling scheme. Errors are of the order of 20%. Where more than one proton was observed in each category, they are listed from the highest to the lowest change observed, regardless of the position in the molecule.
[b] These signals were not sufficiently resolved to obtain reliable chemical-shift changes.

chloroform; one set of experiments used flexible molecules, the other rigid molecules; and one set of experiments focused on structural changes, the other free energy changes. We have examined the CIS data for evidence of structural changes in the zipper system and see no significant differences as the complexes become more stable. In principle, a more rigid molecule should show stronger coupling and enhanced structural tightening compared with a flexible system.

We therefore suggest an alternative form of structural tightening and invoke partially bound states to explain the vancomycin-peptide results (Figure 4). In any complex held together by multiple weak intermolecular interactions, it is possible to populate partially bound states where some of the intermolecular interactions are absent. In effect, there is a free-bound equilibrium for every individual interaction site in the complex. This is different from the global free-bound equilibrium for formation of the complex, but refers to the properties of the bound state that is actually a collection of various different complexed states in equilibrium. In a rigid system, the loss of an interaction site is enthalpically unfavorable, and unless the interaction is very weak, partially bound states will not be populated to any significant extent (Figure 4A). In contrast, for flexible molecules the loss of enthalpy is compensated by a gain in conformational entropy, and partially bound states are expected to be significantly populated (Figure 4B). This explanation leads directly to a rationalization of entropy-enthalpy compensation: in weakly bound complexes, a large part of the available enthalpy is dissipated in the population of entropically favorable partially bound states; in strongly bound complexes, these states are less accessible, but realization of the available enthalpy comes at the entropic cost of freezing out conformational mobility. This is analogous to the situation in short α-helical peptides, where the ends of the helix fray, populating a range of states from structured helicoidal to random coil [32–34].

Application of this concept to the vancomycin-peptide system is illustrated in Figure 4C. The observed variations in CIS values for the vancomycin NH signal can be explained based on changes in the populations of the partially bound states as a function of substrate structure. In effect, the ligand extension experiment titrates out the partially bound states, and so the CIS versus ΔG curve looks very like a standard binding isotherm. The published CIS data suggest that the delicate balance between the entropy gain of freeing up two single-bond rotors and the enthalpic cost of losing interactions with the binding site leads to an equilibrium constant of 0.3 for population of the partially bound state for each amino acid in the chain. This is why cooperative effects are so large in biological systems: the bound state is only marginally more stable than the free state, and so many interactions are required to bring about well-defined structure.

This analysis rationalizes the results from the two sets of experiments. In weakly bound complexes, the population of partially bound states leads to relatively low entropy and enthalpy changes on binding. There is a trade-off between the favorable enthalpy available by maximizing the intermolecular interactions and entropic cost of restricting the conformational freedom of the system. When additional binding interactions are added, the balance between enthalpy and entropy shifts in favor of more interactions and less conformational freedom. The result is structural tightening and enthalpic cooperativity. However, if the enthalpic cooperativity is balanced by the entropic costs, there is no net effect on the free energy. In other words, enthalpic cooperativity does not necessarily translate into free energy cooperativity.

Significance

Cooperativity is a general property of intermolecular interactions, but the origins of the effect remain obscure. Here, we show that in a H-bonded complex of two relatively rigid molecules the individual functional group interactions do not change as the overall stability of a complex increases. At the same time, NMR spectroscopy shows no evidence of structural tightening in the complexes. We conclude that the structural tightening and enthalpic cooperativity observed in other systems is related to conformational flexibility. If the individual interaction sites are linked by flexible chains, as in peptides, the system will populate partially bound states to a significant extent. Thus, not all interactions between the two molecules are made simultaneously, and a substantial fraction of the available enthalpy of intermolecular functional group interactions is distributed as conformational entropy in the

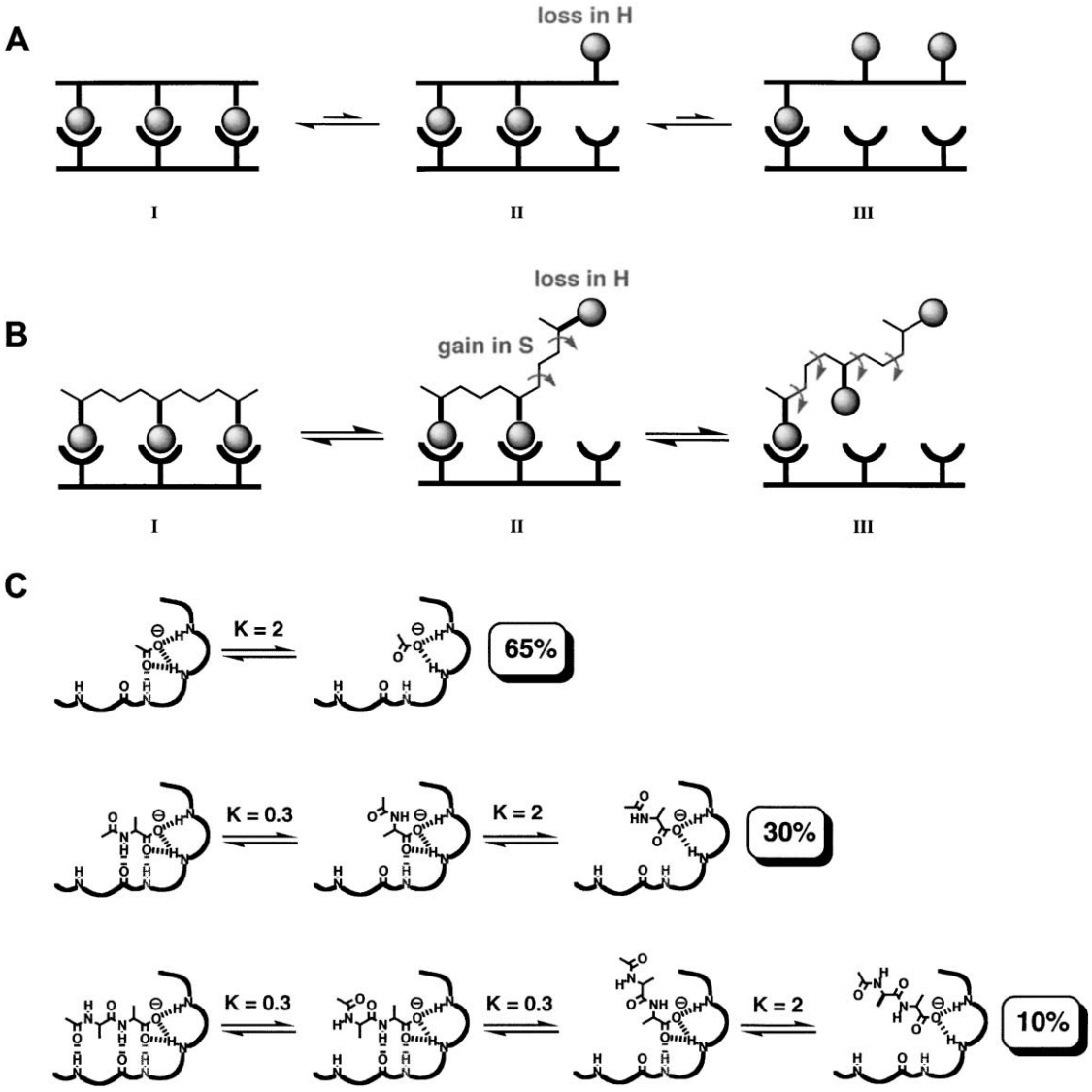

Figure 4. Partially Bound States: Influence in ΔH, ΔS, and the Spectroscopic Properties of Complexes

(A and B) Schematic representation of partially bound states in (A) a rigid complex and (B) a flexible complex. The associated gain in conformational entropy leads to an increase in the population of partially bound states in flexible systems.

(C) The population of partially bound states in vancomicyn-peptide complexes explains the observed variation in the CIS values for the vancomycin NH (gray) as the peptide is extended [13]. The population of the state in which the gray NH is not H bonded and the equilibrium constants are derived from the published CIS data. It is striking that the same equilibrium constant is obtained for each amino acid added to the chain.

flexible chains. This behavior leads to the enthalpy-entropy compensation that is frequently observed in molecular recognition events. These effects are related to the internal structure of the complex and do not relate to changes in the free energy of the system that defines the observed stability.

Experimental Procedures

All chemicals were purchased from the Aldrich Chemical Co. and used without further purification.

Synthesis of 1

9 (1.587 g, 1.517 mM) and Et_3N (0.225 ml, 1.669 mmol) were dissolved in 60 ml of dry CH_2Cl_2. 4-*t*-buthyl benzoyl chloride (0.298 g, 1.517 mmol) in 40 ml of dry CH_2Cl_2 was then added dropwise, and the resulting solution was allowed to stir for 6 hr at room temperature. After that period, Et_3N (0.225 ml, 1.669 mmol) was added to the solution. Then freshly prepared acid chloride **10** (0.264 g, 1.517 mmol) was dissolved in 10 ml of dry CH_2Cl_2 and added dropwise to the reaction mixture. The solution was allowed to stir for 14 hr at room temperature. Then the solvent was removed under reduced pressure, and the crude product was purified by column chromatography on silica using a mixture CH_2Cl_2:MeOH 98:2 v/v as eluent. Two bands were separated. The first one contained oligomer **3** (1.002 g). The second was the desired product (0.387g, 19% yield). ^{1}H NMR ($CDCl_3$/d_6-DMSO): 12.37 (s, 1H), 9.33 (s, 1H), 9.32 (s, 1H), 9.29 (s, 1H), 9.14 (s, 1H), 8.58 (s, 1H), 8.07 (d, J = 7.9 Hz, 2H), 7.84 (d, J = 8.6 Hz, 2H), 7.61 (s, 1H), 7.54 (s, 1H), 7.50 (t, J = 7.8 Hz, 2H), 7.39 (d, J = 8.6 Hz, 2H), 7.26 (m, 10H), 6.96 (s, 2H), 6.95 (s, 4H), 6.93 (s, 2H), 5.02 (s, 4H), 3.50 (br, 8H), 2.32 (br, 8H), 2.22 (s, 6H), 2.16 (s, 6H), 2.13 (s,

6H), 2.07 (s, 6H), 1.26 (s, 9H) ppm. FAB-MS (*m/z*): 1340 [$M - 3H^+$]. Elemental analysis calculated (%) for $C_{82}H_{86}N_8O_{10}\cdot H_2O$: 72.33, 6.51, 8.23; found: 72, 21, 6.71, 8.06.

Synthesis of 2

11 (0.721 g, 0.715 mmol) and Et_3N (0.212 mL, 1.574 mmol) were dissolved in 500 ml of CH_2Cl_2 and added dropwise to a solution of isophthaloyl dichloride (0.912 g, 4.492 mmol) in CH_2Cl_2 (100 ml). The solution was then allowed to stir for 2 hr at room temperature. After this period, freshly prepared 2,6-diisopropyl-*N,N*-dimethyl-benzene-1,4-diamine **12** (2.381 g, 10.82 mmol) and Et_3N (1.458 mL, 10.82 mmol) in CH_2Cl_2 (20 ml) were added dropwise to the reaction mixture. The solution was allowed to stir for 14 hr at room temperature. The solvent was then removed under reduced pressure. Flash column chromatography on silica using a gradient elution with a mixture CH_2Cl_2:MeOH (99.5:0.5 to 98.5:1.5 v/v) allowed the separation of two bands. The first one contained **4** (0.435 g). The second was the desired product **2,** which was obtained as a white solid (0.517 g, 45% yield). ^{1}H NMR ($CDCl_3$/d_6-DMSO): 9.31 (s, 2H), 8.99 (s, 2H), 8.59 (s, 2H), 8.09 (t, J = 7.9 Hz, 4H), 7.51 (t, J = 7.9 Hz, 2H), 6.97 (s, 4H), 6.49 (s, 2H), 6.46 (s, 4H), 3.87 (m, 6H), 3.73 (br, 2H), 3.49 (br, 2H), 3.05 (m, J = 7 Hz, 4H), 3.04 (s, 12H), 2.43 (br, 2H), 2.34 (br, 2H), 2.18 (s, 12H), 1.71 (m, 6H), 1.39 (m, 6H), 1.17 (br, 60H), 1.12 (d, J = 7 Hz, 24H), 0.79 (t, 9H) ppm. ^{13}C NMR ($CDCl_3$): 170.4, 166.5, 165.6, 153.2, 150.6, 146.9, 144.9, 139.2, 136.3, 134.2, 133.8, 132.8, 131.0, 130.9, 128.8, 126.4, 126.0, 120.8, 107.8, 105.4, 73.5, 69.3, 43.7, 40.8, 31.9, 30.3, 29.7–29.4 (multiple signals), 29.1, 26.1, 23.7, 22.7, 18.9, 14.1 ppm. MALDI-TOF MS (*m/z*), 1766 [$M + H^+$]. HRMS, 1765.3052; calculated for $C_{114}H_{170}N_7O_8$, 1765.3111.

Synthesis of 5

13 (1.351g, 2.267 mmol) and Et_3N (0.336 ml, 2.493 mmol) were dissolved in 100 ml of CH_2Cl_2. 4-*t*-buthyl benzoyl chloride (0.491 g, 2.494 mmol) in CH_2Cl_2 (40 ml) was then added dropwise. The solution was allowed to stir 14 hr at room temperature. Then the solvent was removed under reduced pressure. Flash column chromatography on silica using a gradient elution with a mixture CH_2Cl_2:MeOH (99.5:0.5 to 98:2 v/v) allowed the separation of **5**, which was obtained as a white solid (0.406, 24% yield). ^{1}H NMR ($CDCl_3$/d_6-DMSO): 11.98 (s, 1H), 8.89 (s, 1H), 8.86 (s, 1H), 7.46 (d, J = 8.4 Hz, 2H), 7.22 (s, 1H), 7.14 (s, 1H), 7.00 (d, J = 8.4 Hz, 2H), 6.85 (m, 5H), 6.54 (s, 2H), 6.53 (s, 2H), 4.63 (s, 2H), 3.10 (br, 4H), 1.92 (br, 4H), 1.74 (s, 6H), 1.73 (s, 6H), 0.87 (s, 9H) ppm. ^{13}C NMR (d_6-DMSO): 164.9, 157.9, 154.6, 154.3, 145.3, 144.6, 137.0, 136.5, 135.6, 135.5, 133.2, 132.1, 131.6, 128.4, 127.8, 127.5, 127.3, 126.6, 126.0, 125.2, 122.9, 120.6, 105.8, 66.2, 43.5, 40.9, 34.9, 34.6, 30.9, 18.5 ppm. FAB-MS (*m/z*): 756 [$M + H^+$]. Elemental analysis calculated (%) for $C_{45}H_{49}N_5O_6\cdot 1/2H_2O$: 70.70, 6.78, 9.06; found: 70.51, 6.64, 9.29.

Binding Studies

^{1}H NMR dilution experiments were used to determine the dimerization constants of the single components. In a typical experiment, a saturated stock solution of the compound was prepared (0.005–0.05 M). Aliquots of this solution were added to 0.5 ml of $CDCl_3$, and a ^{1}H NMR spectrum was recorded after each addition. The chemical shift of each signal was analyzed using nonlinear curve fitting to fit the data to a dimerization isotherm (*NMRDil_Dimer*) [35]. This procedure optimizes the dimerization constant and the limiting bound and free chemical shifts. A representative data set is illustrated in Figure 5C.

^{1}H NMR titrations were carried out by preparing a 3 ml sample of the host at known concentration (3–4 mM) in $CDCl_3$. 0.5 ml of this solution was removed, and a ^{1}H NMR spectrum was recorded. An accurately weighed sample of the guest was then dissolved in 2 ml of the host solution (so that the concentration of host remained constant during the titration). Aliquots of guest solution were added successively to the NMR tube containing the host solution, and the ^{1}H NMR spectrum was recorded after each addition. Signals that moved more than 0.01 ppm were analyzed using nonlinear curve fitting (*NMRTit_HGHHGG*). *NMRTit_HGHHGG* fits the data to a 1:1 binding isotherm, allowing for dimerization of both binding partners [35]. This procedure optimizes the association constant and the limiting bound chemical shift. A representative data set is illustrated in Figure 5D.

The procedure for ^{1}H NMR dilution experiments on the complexes is identical to that described above for dimerization of single component systems, except that a 1:1 mixture of the two compounds was used, and *NMRDil_HGHHGG* was used to fit the data to a 1:1 binding isotherm, allowing for dimerization of both binding partners [27]. This procedure optimizes the association constant and the limiting bound chemical shift. A representative data set is illustrated in Figure 5E.

All NMR experiments were performed at least twice. The association constant for a single run was calculated as the mean of the values obtained for each of the signals followed during the titration weighted by the observed changes in chemical shift. The association constants from different runs were then averaged. Errors are quoted at the 95% confidence limits (twice the standard error). For a single run, the standard error was determined using the standard deviation of the different association constants determined by following different signals. The curve-fitting programmes are available from the author on request.

ITC experiments were performed on a VP-ITC Microcal Calorimeter. To study dimerization of the individual components, the compound was dissolved in HPLC grade $CHCl_3$ with a concentration 10–100 times the expected dissociation constant and loaded into the injection syringe. Pure solvent was loaded into the sample cell of the microcalorimeter. The number of injections was between 50–80, and the volume of the injection was between 3–8 μl. The thermogram peaks were integrated using Microcal Origin V 5.0, and the resulting data were fit to a dimerization isotherm using purpose-written software on an Apple Macintosh microcomputer, *ITCDil_Dimer*. This program use a Simplex procedure to fit the experimental data to the following equations to determine the optimum solutions for the association constant and the enthalpy of dimerization. A representative data set is illustrated in Figure 5A.

$$[AA] = \frac{1 + 4K_d[A]_0 - \sqrt{\{1 + 8K_d[A]_0\}}}{8K_d} \quad (1)$$

$$[A] = [A]_0 - 2[AA], \quad (2)$$

where $[A]_0$ is the total concentration, [A] is the concentration of unbound species, [AA] is the concentration of dimer, and K_d is the dimerization constant.

For each injection:

$$Q_i = Q_0 + \frac{2\Delta H_d\{V([AA]^c_i - [AA]^c_{i-1}) + V_i([AA]^c_{i-1} - [AA]^s)\}}{V_i[A]^s_0}, \quad (3)$$

where Q_i is the integrated molar heat of the i-th injection, Q_0 is a baseline correction factor that is usually of the order 1 kJ mol^{-1}, ΔH_d is the enthalpy of dimerization per mole of monomer, V is the volume of the cell (1428.7 μl), V_i is the volume of the i-th injection, $[A]^s_0$ is the total concentration in the syringe, $[AA]^s$ is the concentration of dimer in the syringe, and $[AA]^c_{i-1}$ and $[AA]^c_i$ are the concentrations of dimer in the cell before and after the i-th injection.

In a typical ITC titration experiment, one of the components of the complex was dissolved in HPLC grade $CHCl_3$ with a concentration 10–100 times the expected dissociation constant, and the solution was loaded into the sample cell of the microcalorimeter. A solution of the second component 8–10 times more concentrated than the cell solution was loaded into the injection syringe. The number of injections was between 50–80, and the volume of the injection was between 3–8 μl. The thermogram peaks were integrated using Microcal Origin V 5.0, and the resulting data were fit to a 1:1 binding isotherm using purpose-written software on an Apple Macintosh microcomputer, *ITCTit_HG_HH_GG*. This program requires a previous determination of the dimerization parameters (K_d and ΔH_d) for the two components and fits the data to a 1:1 binding isotherm, taking into account the dimerization equilibria for both the host and guest.

The component in the cell is defined as host (H) and the component in the syringe as guest (G). The method starts by assuming that [HG] = 0, so that Equations 5 and 6 can be solved exactly for

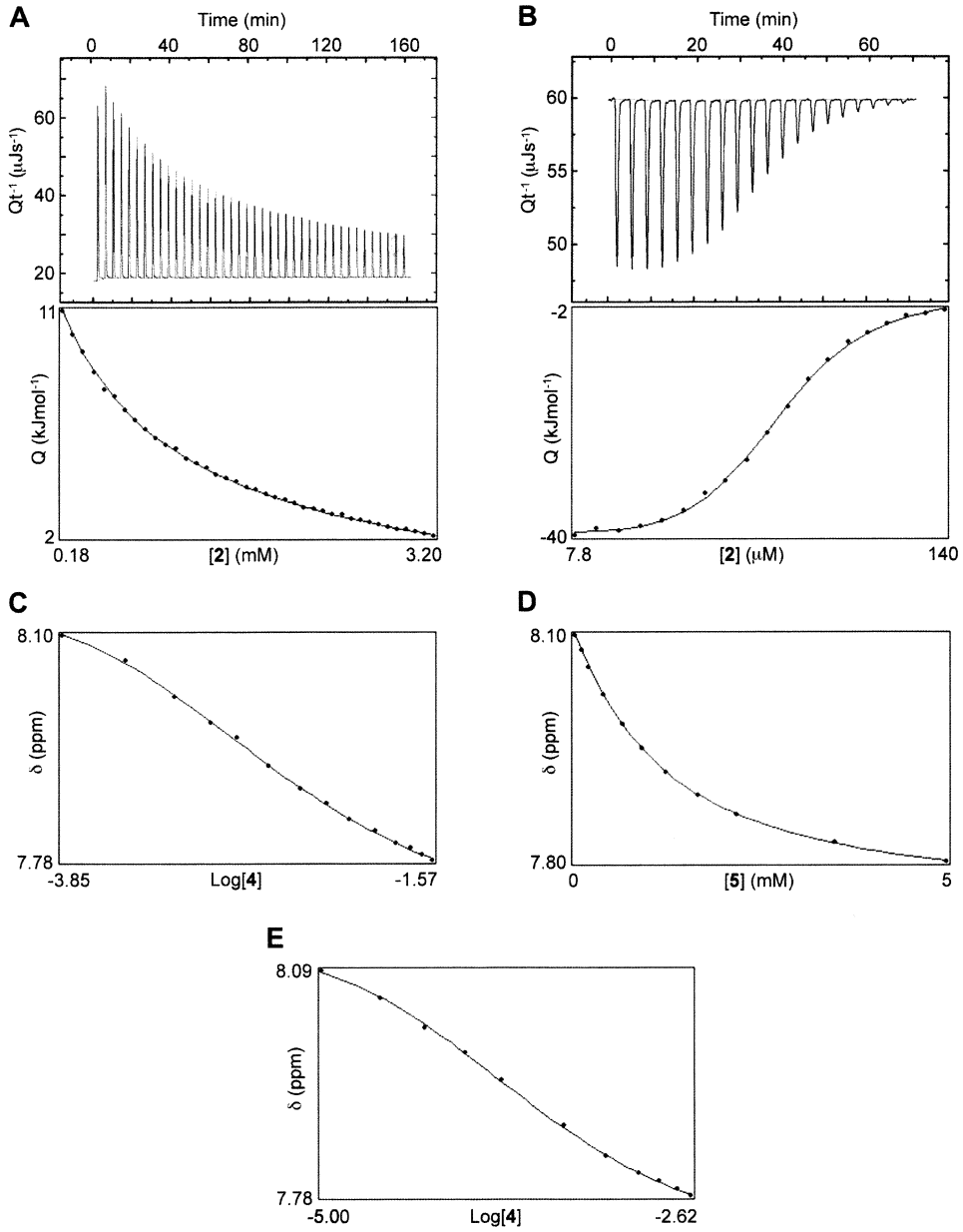

Figure 5. ITC and NMR Titration Data

(A) ITC data for dilution of compound **2** in $CHCl_3$ at 294 K. The thermogram is shown in the upper panel, and the fit of the integrals of the peaks to a dimerization isotherm is shown in the lower panel.

(B) ITC data for titration of compound **2** into compound **1** in $CHCl_3$ at 294 K. The thermogram is shown in the upper panel, and the fit of the integrals of the peaks to a 1:1 binding isotherm that allows for dimerization of both components is shown in the lower panel.

(C) ^1H NMR dilution data for proton j in compound **4** recorded in $CDCl_3$ at 294 K. The curve shows the fit to the dimerization isotherm. The data span 10%–81% bound and were used to determine the bound and free chemical shifts and the dimerization constant.

(D) ^1H NMR titration data for proton j in compound **6** on addition of compound **5** in $CDCl_3$ at 294 K. The curve shows the fit to the 1:1 binding isotherm that allows for dimerization of both compounds. The data span 0%–75% bound and were used to determine the bound chemical shift and the association constant.

(E) ^1H NMR dilution data for a 1:1 mixture of **3** and **4** recorded in $CDCl_3$ at 294 K showing the data for proton j in compound **4**. The curve shows the fit to the 1:1 binding isotherm that allows for dimerization of both compounds. The data span 7%–83% bound and were used to determine the bound and free chemical shifts and the dimerization constant.

[HH] and [GG]. These values are then used to solve Equation 7 for [HG]. Equations 8 and 9 give the concentrations of free host [H] and free guest [G]. At this point, $[H] + [HH] + [HG] \neq [H]_0$, and $[G] + [GG] + [HG] \neq [G]_0$, so the value of [HG] from Equation 7 is used in Equations 5 and 6 to reevaluate [HH] and [GG], and the procedure is carried out repetitively until $[H] + [HH] + [HG] = [H]_0$ and $[G] + [GG] + [HG] = [G]_0$. This allows the set of simultaneous equations to be solved for the concentrations of all species present.

$$[H]_0 = n[H]^c_0 \quad (4)$$

$$[HH] = \frac{1 + 4K_{dH}([H]_0 - [HG]) - \sqrt{\{1 + 8K_{dH}([H]_0 - [HG])\}}}{8K_{dH}} \quad (5)$$

$$[GG] = \frac{1 + 4K_{dG}([G]_0 - [HG]) - \sqrt{\{1 + 8K_{dG}([G]_0 - [HG])\}}}{8K_{dG}} \quad (6)$$

$$[HG] = \frac{1 + K_a([G]_0 - [GG])([H]_0 - [HH] - \sqrt{\{(1 + K_a([G]_0 - [GG])([H]_0 - [HH]))^2 - 4K_a^2([G]_0 - [GG])([H]_0 - [HH])\}}}{2K_a} \quad (7)$$

$$[H] = [H]_0 - 2[HH] - [HG] \quad (8)$$

$$[G] = [G]_0 - 2[GG] - [HG], \quad (9)$$

where $[H]^c_0$ is the total concentration of host in the cell, $[H]_0$ is the concentration of host binding sites, n is the number of binding sites on the host and is usually very close to one, $[G]_0$ is the total concentration of guest, [HH] is the concentration of host dimer, [GG] is the concentration of guest dimer, K_{dH} is the dimerization constant of the host, K_{dG} is the dimerization constant of the guest, and K_a is the host-guest association constant.

For each injection:

$$Q_i = Q_0 + \frac{Q_{HG} + Q_{HH} + Q_{GG}}{V_i[G]^s_0}, \quad (13)$$

where

$$Q_{GG} = 2\Delta H^G_d\{V([GG]_i - [GG]_{i-1}) + V_i([GG]_{i-1} - [GG]^s)\} \quad (10)$$

$$Q_{HH}\ 2\Delta H^H_d\ \{V([HH]_i - [HH]_{i-1}) + V_i[HH]_{i-1}\} \quad (11)$$

$$Q_{HG} = \Delta H_a\{V([HG]_i - [HG]_{i-1}) + V_i[HG]_{i-1}\}, \quad (12)$$

ΔH^H_d and ΔH^G_d are the enthalpies of dimerization per mole of monomer of the host and guest, respectively, ΔH_a is the molar enthalpy for formation of the host-guest complex, $[G]^s_0$ is the total concentration in the syringe, $[GG]^s$ is the concentration of dimer in the syringe, $[GG]^c_{i-1}$ and $[GG]^c_i$ are the concentrations of guest dimer in the cell before and after the i-th injection, $[HH]^c_{i-1}$ and $[HH]^c_i$ are the concentrations of host dimer in the cell before and after the i-th injection, and $[HG]^c_{i-1}$ and $[HG]^c_i$ are the concentrations of host-guest complex in the cell before and after the i-th injection.

All experiments were performed at least twice. The association constants from different runs were then averaged. Errors are quoted at the 95% confidence limits (twice the standard error). A representative data set is illustrated in Figure 5B.

Acknowledgments

We thank the BBSRC (ST) and the Lister Institute (CAH) for funding.

Received: March 6, 2003
Revised: July 29, 2003
Accepted: August 18, 2003
Published: November 21, 2003

References

1. Jencks, W.P. (1981). On the attribution and additivity of binding energies. Proc. Natl. Acad. Sci. USA *78*, 4046–4050.
2. Jencks, W.P. (1975). Binding energy, specificity, and enzymic catalysis: the circe effect. Adv. Enzymol. Relat. Areas Mol. Biol. *43*, 219–410.
3. Martell, A.E. (1964). In Essays in Coordination Chemistry, W. Schneider, G. Anderegg, and R. Gutt, eds. (Basel: Birkhauser), p. 52.
4. Adamson, A.W. (1954). A proposed approach to the chelate effect. J. Am. Chem. Soc. *76*, 1578–1579.
5. Schwarzenbach, G. (1952). The chelate effect. Helv. Chim. Acta *35*, 2344–2359.
6. Albeck, S., Unger, R., and Schreiber, G. (2000). Evaluation of direct and cooperative contributions towards the strength of buried hydrogen bonds and salt bridges. J. Mol. Biol. *298*, 503–520.
7. Griffiths-Jones, S.R., and Searle, M.S. (2000). Structure, folding, and energetics of cooperative interactions between the β-strands of a *de novo* designed three-stranded antiparallel β-sheet peptide. J. Am. Chem. Soc. *122*, 8350–8356.
8. Schreiber, G., Frisch, C., and Fersht, A.R. (1997). The role of Glu73 of barnase in catalysis and the binding of barstar. J. Mol. Biol. *270*, 111–122.
9. Mackay, J.P., Gerhard, U., Beauregard, D.A., Maplestone, R.A., and Williams, D.H. (1994). Dissection of the contributions toward dimerization of glycopeptide antibiotics. J. Am. Chem. Soc. *116*, 4573–4580.
10. Horovitz, A., and Fersht, A.R. (1992). Cooperative interactions during protein folding. J. Mol. Biol. *224*, 733–740.
11. Horovitz, A., and Fersht, A.R. (1990). Strategy for analyzing the cooperativity of intramolecular interactions in peptides and proteins. J. Mol. Biol. *214*, 613–617.
12. Prince, R.B., Saven, J.G., Wolynes, P.G., and Moore, G.S. (1999). Cooperative conformational transitions in phenylene ethylene oligomers: chain-length dependence. J. Am. Chem. Soc. *121*, 3114–3121.
13. Bisson, A.P., and Hunter, C.A. (1996). Cooperativity in the assembly of zipper complexes. Chem. Commun. (Camb.) 1723–1724.
14. Pfeil, A., and Lehn, J.-M. (1992). Helicate self-organization: positive cooperativity in the self-assembly of double-helical metal complexes. J. Chem. Soc. Chem. Commun. 838–840.
15. Williams, D.H., Gale, T.F., and Bardsley, B. (1999). The increasing tightness of fully associated states as a function of their increasing stability. The dimerization of carboxylic acids. J. Chem. Soc. [Perkin 1] *7*, 1331–1334.
16. Williams, D.H., Maguire, A.J., Tsuzuki, W., and Westwell, M.S. (1998). An analysis of the origins of a cooperative binding energy of dimarization. Science *280*, 711–714.
17. Searle, M.S., Sharman, G.J., Groves, P., Benhamu, B., Beauregard, D.A., Westwell, M.S., Dancer, R.J., Maguire, A.J., Try, A.C., and Williams, D.H. (1996). Enthalpic (electrostatic) contribution to the chelate affect: a correlation between ligand binding constant and a specific hydrogen bond strength in complexes of glycopeptide antibiotics with cell wall analogs. J. Chem. Soc. [Perkin 1] *23*, 2781–2786.
18. Groves, P., Searle, M.S., Westwell, M.S., and Williams, D.H. (1994). Expression of electrostatic binding cooperativity in the recognition of cell-wall peptide analogs by vancomycin group antibiotics. J. Chem. Soc. Chem. Commun. 1519–1520.
19. Williams, D.H., O'Brian, D.P., and Bardsley, B. (2001). Enthalpy/entropy compensation as a competition between dynamics and bonding: the relevance to melting of crystals and biological aggregates. J. Am. Chem. Soc. *123*, 737–738.
20. Williams, D.H., and Westwell, M.S. (1998). Aspects of weak interactions. Chem. Soc. Rev. *27*, 57–63.
21. Westwell, M.S., Searle, M.S., Klein, J., and Williams, D.H. (1996). Successful predictions of the residual motion of weakly associated species as a function of the bonding between them. J. Phys. Chem. *100*, 16000–16001.
22. Searle, M.S., Wetswell, M.S., and Williams, D.H. (1995). Application of a generalised enthalpy-entropy relationship to binding co-operativity and weak associations in solution. J. Chem. Soc. [Perkin 1] *2*, 141–151.
23. Adams, H., Hunter, C.A., Lawson, K.R., Perkins, J., Spey, S.E., Urch, C.J., and Sanderson, J.M. (2001). A supramolecular system for quantifying aromatic stacking interactions. Chemistry *7*, 4863–4877.
24. Adams, H., Jimenez-Blanco, J.L., Chesari, G., Hunter, C.A., Low, C.M.R., Sanderson, J.M., and Vinter, J.G. (2001). Quantitative determination of intermolecular interactions with fluorinated aromatic rings. Chemistry *7*, 3494–3503.

25. Carver, F.J., Hunter, C.A., Jones, P.S., Livingstone, D.J., McCabe, J.F., Seward, E.M., Tiger, P., and Spey, S.E. (2001). Quantitative measurements of edge-to-face aromatic interactions by using chemical double-mutant cycles. Chemistry *7*, 4854–4862.
26. Carver, F.J., Hunter, C.A., Livingstone, D.J., McCabe, J.F., and Seward, E.M. (2002). Substituent effects on edge-to-face aromatic interactions. Chemistry *8*, 2847–2859.
27. Hunter, C.A., Jones, P.S., Tiger, P., and Tomas, S. (2002). Chemical triple-mutant boxes for quantifying cooperativity in intermolecular interactions. Chemistry *8*, 5435–5446.
28. Jusuf, S., Loll, P.J., and Axelsen, P.H. (2002). The role of configurational entropy in biochemical cooperativity. J. Am. Chem. Soc. *124*, 3490–3491.
29. Shiozawa, H., Chia, B.C.S., Davies, N.L., Zerella, R., and Williams, D.H. (2002). Cooperative binding interactions of glycopeptide antibiotics. J. Am. Chem. Soc. *124*, 3914–3919.
30. Rao, J., Lahiri, J., Weis, R.M., and Whitesides, G.M. (2000). Design, synthesis, and characterisation of a high-affinity trivalent system derived from vancomycin and L-lys-D-ala-D-ala. J. Am. Chem. Soc. *122*, 2698–2710.
31. Taylor, P.N., and Anderson, H.L. (1999). Cooperative self-assembly of double-strand conjugated porphyrin ladders. J. Am. Chem. Soc. *121*, 11538–11545.
32. Zhang, Y.-P., Lewis, R.N.A.H., Henry, G.D., Sykes, B.D., Hodges, R.S., and McElhaney, R.N. (1995). Peptide models of helical hydrophobic transmembrane segments of membrane proteins. 1. Studies of the conformation, intrabilayer orientation, and amide hydrogen exchangeability of Ac-K2-(LA)12–K2-amide. Biochemistry *34*, 2348–2361.
33. Muroga, Y., Muraki, T., Noda, I., Tagawa, H., Holtzer, A., and Holtzer, M.E. (1995). Chain unfolding equilibria of α-tropomyosin coiled coils studied by small angle X-ray scattering. J. Am. Chem. Soc. *117*, 5622–5626.
34. Rhol, C.A., and Baldwin, R.L. (1994). Exchange kinetics of individual amide protons in ^{15}N-labeled helical peptides measured by isotope-edited NMR. Biochemistry *33*, 7760–7767.
35. Bisson, A.P., Carver, F.J., Eggleston, S., Haltiwanger, R.C., Hunter, C.A., Livingstone, D.L., McCabe, J.F., Rotger, C., and Rowan, A.E. (2000). Synthesis and recognition properties of aromatic amide oligomers: molecular zippers. J. Am. Chem. Soc. *122*, 8856–8868.